Desalination and Water Treatment
www.deswater.com

doi: 10.5004/dwt.2022.28444

259 (2022) 71–81
May

Fe_2O_3/g-C_3N_4/CNTs based nanocomposites incorporated with neodymium and samarium nanoparticles for efficient photocatalytic vitiation of organic pollutants

Nosheen Farooq[a,b], Muhammad Imran Khan[c,*], Ashfaq Mahmood Qureshi[b], Muhammad Ahmad Wattoo[d], Abdallah Shanableh[c], Saima Anjum[b], Aziz ur Rehman[a,*]

[a]*Institute of Chemistry, The Islamia University of Bahawalpur, Bahawalpur 63100, Pakistan, emails: draziz@iub.edu.pk/azizypk@yahoo.com (Aziz ur Rehman), nosheen.farooq@gscwu.edu.pk (N. Farooq)*
[b]*Department of Chemistry, The Government Sadiq College Women University, Bahawalpur 63100, Pakistan, ashfaq.qureshi@gscwu.edu.pk (A.M. Qureshi), drsaima@gscwu.edu.pk (S. Anjum)*
[c]*Research Institute of Sciences and Engineering (RISE), University of Sharjah, Sharjah 27272, United Arab Emirates, email: raoimranishaq@gmail.com/mimran@sharjah.ac.ae (M.I. Khan), Shanableh@sharjah.ac.ae (A. Shanableh)*
[d]*Department of Chemistry, Quaid-e-Azam University, Islamabad, Pakistan, email: ahmadwattoo@yahoo.com (M.A. Wattoo)*

Received 17 December 2021; Accepted 27 March 2022

ABSTRACT

Neodymium and samarium based nanocomposites with efficient photocatalytic activity were synthesized and their structural and morphology were characterized using Fourier-transform infrared spectroscopy, X-ray diffraction, scanning electron microscopy (SEM) and energy-dispersive X-ray spectroscopy techniques. The SEM results of synthesized nanocomposites depict the flaked morphology of graphitic carbon nitride with interlinked stacked structure of metallic framework. UV-visible spectral studies revealed that the absorption edge has been shifted to longer wavelength in samarium and neodymium based samples which results in the decreased band gap of g-C_3N_4 being used as main precursor. The photocatalytic activity of the synthesized catalysts was assessed by studying the degradation of Rhodamine B and Congo red dyes under visible light. The obtained results depict that Fe_2O_3/g-C_3N_4/CNTs/Sm_2O_3 nanocomposite is more efficient with 86.1% degradation efficiency and 80.2% for Rhodamine B and Congo red as compared to Fe_2O_3/g-C_3N_4/CNTs/Nd_2O_3. Present studies revealed that superoxide ions and holes play significant role in the degradation of dye effluents. Further, the possible mechanism of the photocatalytic degradation of pollutants using samarium based nanocomposites is also proposed.

Keywords: Graphitic carbon nitride; CNTs; Neodymium; Samarium; Photocatalytic activity

1. Introduction

The entire world is facing the problems of pollution caused by rapid increase in numbers of industries, due to which living organisms especially human beings are badly affected. For this purpose, a lot of ways are adopted for degradation of harmful pollutants using economical materials. For this purpose, researchers are keenly devoted for using efficient and eco-friendly materials as tool of cleaning major water bound pollutants. The choice of materials is focused on smaller sized large surface area with-holding properties.

Owing to innumerable properties like simple preparation, high chemical stability, use of visible light as source,

* Corresponding authors.

1944-3994/1944-3986 © 2022 Desalination Publications. All rights reserved.

low cost of the material and non-toxicity, graphitic carbon nitride (g-C_3N_4) has been selected as a photo catalyst of choice [1,2]. The two dimensional (2D) graphitic carbon nitride (g-C_3N_4) is an example of n-type semiconductor with a moderate band gap of 2.7 eV which causes it to absorb a narrow range of visible light [3].

Due to the appropriate valence Band (VB) and conduction band (CB) potential energy, Graphitic C_3N_4 is widely accepted as photo catalyst for hydrogen production [4]. As compared to g-C_3N_4, CB band of metal oxides (ZnO) possesses lower energy. Hence the application of Sm doped-ZnO and g-C_3N_4 could exert high photo activity due to their synergistic effect and proper matching of valence band (VB) and conduction band (CB) potential which could allow higher charge separation through the heterojunction [5,6]. Graphite carbon nitride polymer has a special electronic structure and is corresponding to graphite, which has resulted in the use of this material in optical sensor, light emitting devices and photo cathodes [7]. It can also be used as a visible-light-responsive and metal free photo catalyst in solar energy conversion field [8].

Fe_2O_3 has been widely used as an improved semiconducting material with average band gap of about 2.1 eV, excessively used as visible light driven photocatalyst but with short lifetime of excited state and high recombination rate of electron hole pairs. For this deficient nature, Fe_2O_3 has been combined with g-C_3N_4 as Fe_2O_3/g-C_3N_4 to utilize the maximum efficiency of both materials in the field of photocatalysis [9,10].

Rare earth metals have been utilized in broad applications owing to suitability for sensors, solar cells, nano-optics, semiconductors and catalytic activities. Neodymium oxide (Nd_2O_3) is naturally abundant, important and highly reactive element in the series of rare earth metal oxides [11,12]. Nd_2O_3 has numerous uses in dielectrics, magnetic devices and catalysts, to improve the electrical properties of materials [13]. Whereas samarium oxide due to the exceptional properties of lowered crystallite size, increased surface area; enhanced separation efficiency of charge carriers, lowering the band gap and availability of 4f level improves the performance of composite when incorporated [14].

CNTs have been used from last few decades due to their exceptional structural and fabricating properties, providing large number of spaces and surface area for better applications. In recent researches, metal oxides linked CNTs are being used in the fields of photocatalysis [15]. M_2O_3/CNTs have been synthesized in this work and then attachment with g-C_3N_4/Fe_2O_3 nanomaterial has been done as a different approach for studying photocatalytic degradation of dyes as application.

2. Experimental work

2.1. Materials used

The chemicals used for this work were all of analytical grade and no further purification was needed before their usage. Major chemicals being used are listed as; urea (CH_4N_2O) (Sigma-Aldrich, USA), carbon nanotubes (CNTs) (Sigma-Aldrich), neodymium nitrate hexahydrate ($Nd(NO_3)_3{\cdot}6H_2O$), samarium nitrate hexahydrate ($Sm(NO_3)_3{\cdot}6H_2O$), ferrous sulphate heptahydrate ($FeSO_4{\cdot}7H_2O$) (Sigma-Aldrich, USA), polyethylene glycol (PEG) (Sigma-Aldrich, USA), cetyl trimethyl ammonium bromide (CTAB) (Sigma-Aldrich, USA), distilled and deionized water for preparation of solutions and washing purposes.

2.2. Method of synthesis

2.2.1. Synthesis of Fe_2O_3 nanoparticles

The Fe_2O_3 nanoparticles were synthesized with little modification, by using basic media of NaOH, PEG and CTAB as surfactant. 0.1 mol/L $FeSO_4{\cdot}7H_2O$ (2 g/50 mL), solution was prepared using deionised water. NaOH solution of 0.6 mol/L (1.2 g/50 mL) was slowly poured drop wise with continuous stirring until the pH was set to 9. Meanwhile drop wise addition of 1% PEG solution (aqueous) along with 0.1% CTAB solution, to confirm the preparation of iron oxide nanoparticles [16]. The constant stirring at 100°C was ensured for 6 h. Nanoparticles formed were washed thoroughly with distilled water many times in order to remove extra base.

2.2.2. Synthesis of carbon nitride (g-C_3N_4)

The preparation of graphitic carbon nitride was carried out by using thermal exfoliation method. First, about 20 g of urea was put in alumina crucible, covered with lid and then placed in muffle furnace with heating at 550°C for 4.5 h. The graphitic carbon nitride was obtained in the form of yellowish white amorphous flakes, which was first cooled at room temperature followed by grinding using pistol and mortar [17].

2.2.3. Synthesis of Sm_2O_3 and Nd_2O_3 nanoparticles

Neodymium oxide and samarium oxide nanoparticles were separately prepared by using simple sonication method. 1.5 g of neodymium nitrate and samarium nitrate were separately dissolved in 20 mL of distilled water with constant stirring, followed by addition of 30% liquid ammonia. Then sonication was carried out for 35 min to obtain pale coloured samarium hydroxide precipitates and violet coloured neodymium hydroxide precipitates respectively [18,19]. Washing of obtained precipitates was done many times using ethanol and distilled water. The products obtained were annealed at 300°C for 1 h to get M_2O_3 nanoparticles where M = Nd, Sm.

2.2.4. Synthesis of Fe_2O_3/g-C_3N_4/CNTs/Nd_2O_3 and Fe_2O_3/g-C_3N_4/CNTs/Sm_2O_3

Two steps were taken for preparation of Fe_2O_3/g-C_3N_4 and CNTs/M_2O_3 (M = Nd, Sm). Firstly, iron oxide nanoparticles and graphitic carbon nitride were mixed together using simple dispersion and sonication methods. Mixing and sonication was continued for 30 min till homogeneity of mixture was ensured [20]. In the second-step, ultra-sonication was adopted for the formation of CNTs/Nd_2O_3 and CNTs/Sm_2O_3 one by one. 0.8 g of Nd_2O_3 and

Sm_2O_3 nanoparticles were dispersed separately in double distilled water followed by addition of 1.5 mL CNTs (solution) with constant sonication for 1.5 h [21].

Fe_2O_3/g-C_3N_4 in solution form was then mixed with CNTs/Nd_2O_3 and CNTs/Sm_2O_3 separately, followed by sonication for almost 3 h. The products formed were dried by placing in drying oven maintained at 90°C until complete drying of solvent was ensured to get powdered materials. The step by step synthesis process is shown in Fig. 1.

2.2.5. Characterization

X-ray diffraction (XRD) of prepared samples were done by using PANalytical X'Pert Pro MPD Netherland, with Cu Kα radiation having scanning rate 0.005, 30 mA and 35 kV at room temperature (The Islamia University Bahawalpur). The FTIR of all prepared samples was characterized through Alpha Bruker ATR with OPUS/Mentor software (400–4,000cm^{-1}) (The Islamia University Bahawalpur). UV-Visible spectra of prepared samples were obtained using Agilent Carry 60 UV/Visible spectrophotometer (The Government Sadiq Women University Bahawalpur) and scanning electron microscopy (SEM)/energy-dispersive X-ray spectroscopy (EDX) images were obtained using VEGA TESCAN SEM instrument and JEOL JCM-6000 Plus electron microscope (Institute of space Technology Islamabad).

3. Results and discussion

3.1. Fourier-transform infrared spectroscopy

Fourier-transform infrared spectroscopy (FTIR) spectrums of Fe_2O_3/g-C_3N_4/CNTs/Nd_2O_3 and Fe_2O_3/g-C_3N_4/CNTs/Sm_2O_3 have been shown in Fig. 2a and b. Some common bands are available in both of the synthesized materials owing to presence of graphitic carbon nitride, iron oxide and CNTs as same precursors. Elucidation of FTIR peaks of neodymium based materials represents band of 423 cm^{-1} due to vibrational mode of Nd–O group, 668 cm^{-1} band arises due to –OH group attached metal of Nd–OH [22]. The wide peak at 870 cm^{-1} is because of iron oxide presence within composite [23], while other bands at 2,373 cm^{-1} represents C=N bond, 2,943 cm^{-1} for C–H stretching vibrations, band at 3,467 cm^{-1} is for OH stretching due to adsorbed water molecules and stretching vibrations of

Table 1a
Photocatalytic degradation of RhB using Fe_2O_3/C_3N_4/CNTs/Nd_2O_3 NC

Sr #	Time 't' (min)	Initial absorbance A_o	Absorbance at 't' time A_t	% D
1.	0	1.95	1.95	0
2.	5	1.95	1.73	11.28
3.	10	1.95	1.62	16.92
4.	15	1.95	1.56	20
5.	20	1.95	1.43	26.7
6.	25	1.95	1.25	35.9
7.	30	1.95	1.07	45.12
8.	35	1.95	0.90	53.8
9.	40	1.95	0.73	62.6
10.	45	1.95	0.61	68.71
11.	50	1.95	0.48	75.38

Table 1b
Photocatalytic degradation of RhB using Fe_2O_3/C_3N_4/CNTs/Sm_2O_3 NC

Sr #	Time 't' (min)	Initial absorbance A_o	Absorbance at 't' time A_t	% D
1.	0	1.95	1.95	0
2.	5	1.95	1.70	12.82
3.	10	1.95	1.51	22.56
4.	15	1.95	1.37	29.74
5.	20	1.95	1.23	36.92
6.	25	1.95	1.11	43.07
7.	30	1.95	0.95	51.28
8.	35	1.95	0.81	58.46
9.	40	1.95	0.68	65.12
10.	45	1.95	0.53	72.82
11.		1.95	0.27	86.15

Table 1c
Photocatalytic degradation of CR using $Fe_2O_3/C_3N_4/CNTs/Nd_2O_3$ NC

Sr #	Time '*t*' (min)	Initial absorbance A_o	Absorbance at '*t*' time A_t	% *D*
1.	0	1.87	1.87	0.0
2.	5	1.87	1.73	7.5
3.	10	1.87	1.57	16.04
4.	15	1.87	1.49	20.32
5.	20	1.87	1.40	25.13
6.	25	1.87	1.29	31.01
7.	30	1.87	1.19	36.36
8.	35	1.87	1.10	41.17
9.	40	1.87	0.96	48.66
10.	45	1.87	0.87	53.47
11.	50	1.87	0.69	63.10

Table 1d
Photocatalytic degradation of CR using $Fe_2O_3/C_3N_4/CNTs/Sm_2O_3$ NC

Sr #	Time '*t*' (min)	Initial absorbance A_o	Absorbance at '*t*' time A_t	% *D*
1.	0	1.87	1.87	0
2.	5	1.87	1.60	14.43
3.	10	1.87	1.47	21.39
4.	15	1.87	1.26	32.62
5.	20	1.87	0.95	49.19
6.	25	1.87	0.87	53.47
7.	30	1.87	0.79	57.75
8.	35	1.87	0.71	62.03
9.	40	1.87	0.58	68.98
10.	45	1.87	0.44	76.47
11.	50	1.87	0.38	80.21

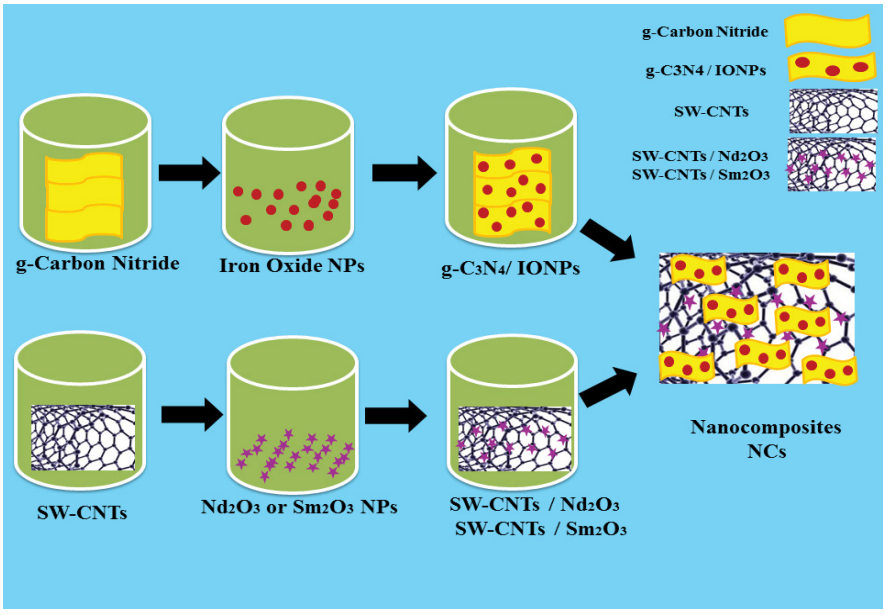

Fig. 1. Pictorial illustration for the synthesis of (i) $Fe_2O_3/g\text{-}C_3N_4/CNTs/Nd_2O_3$ NCs and (ii) $Fe_2O_3/g\text{-}C_3N_4/CNTs/Sm_2O_3$ NCs.

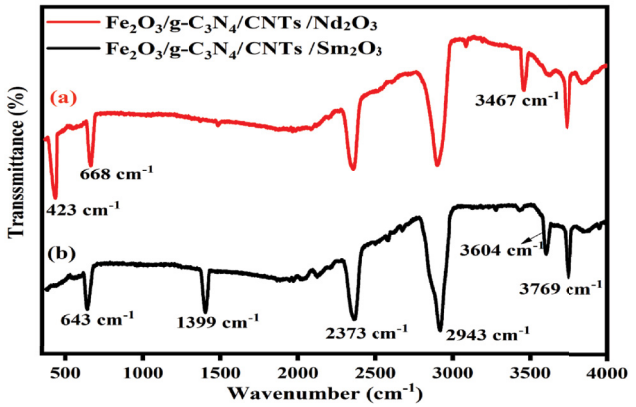

Fig. 2. FTIR of (a) Fe_2O_3/g-C_3N_4/CNTs/Nd_2O_3 NC and (b) Fe_2O_3/g-C_3N_4/CNTs/Sm_2O_3 NC.

NH_2 groups available in g-C_3N_4 framework showing band at 3,769 cm^{-1} respectively [24]. However, the FTIR spectra for Fe_2O_3/g-C_3N_4/CNTs/Sm_2O_3 composite shows some major peaks of 643 cm^{-1} due to Sm–O functional group present [25], while the stretching mode of C–N heterocycles has been shown with band at 1,399 cm^{-1} respectively. The peaks of 870; 2,373; 2,943 and 3,769 cm^{-1} are same as peaks available in Fe_2O_3/g-C_3N_4/CNTs/Nd_2O_3 which correspond to iron oxide, C=N bond, stretching vibrations of C–H groups and stretching vibrations of NH_2 groups respectively. The FTIR peak of 3,604 cm^{-1} is correlated to stretching vibrations of amino groups present on carbon nitride material.

3.2. X-ray diffraction

XRD pattern of Fe_2O_3/g-C_3N_4/CNTs/Nd_2O_3 is shown in Fig. 3a. It depicts peaks of respective precursors used for synthesizing the composite as; XRD peaks with 2θ values of 19.5° and 26.1° with indexed values of (113) and (002) confirm the presence of carbon nanotubes [26], while peaks at 27.7°, 57.1° and 62.9° with hkl values of (002), (428) and (203) correlate g-C_3N_4 within composite [27]. Whereas, peaks with diffraction angle of 33.4° and 35.5° indexed as (207) and (119) are related to Fe_2O_3 nanoparticles [16]. Neodymium oxide (Nd_2O_3) shows the XRD peaks of 30.1°, 47.2° and 53.8° with hkl values of (101), (110) and (103) respectively [28].

The diffraction pattern of Fe_2O_3/g-C_3N_4/CNTs/Sm_2O_3 in Fig. 3b can be elucidated as common peaks of CNTs at 19.5° (113) and 23.4° (002), whereas common peaks of Fe_2O_3 at 33.4° (207) 35.5° (119) and for g-C_3N_4 with peaks of 27.7° (002), 57.1° (428) and 62.9 (203) are also in accordance with that of neodymium based material. While samarium oxide (Sm_2O_3) shows diffraction pattern with peaks at 38.1°, 46.4° and 53.9° along with (332), (521) and (541) hkl values respectively [28,29]. Thus the XRD patterns confirm successful synthesis, showing all precursors with definite diffraction patterns.

3.3. SEM and EDX analyses

The SEM micrographs for neodymium and samarium based nanocomposite are of Fig. 4a and b. The silky

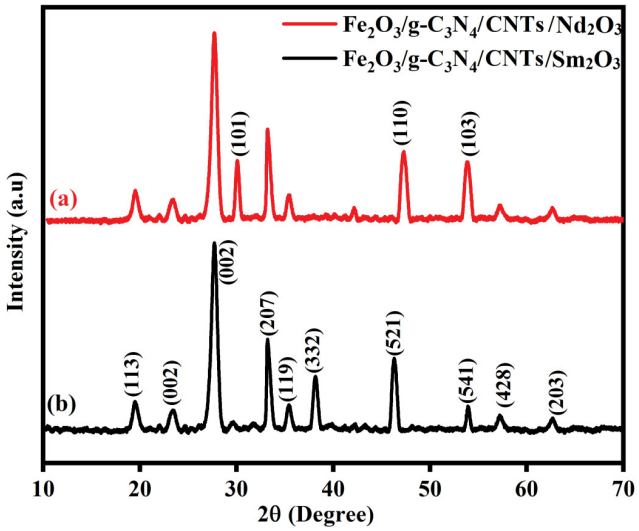

Fig. 3. XRD of (a) Fe_2O_3/g-C_3N_4/CNTs/Nd_2O_3 NC and (b) Fe_2O_3/g-C_3N_4/CNTs/Sm_2O_3 NC.

nanostructures and a layered, flaky sheet like surface morphology are shown by images of 1 and 2 μm scale chosen, which indicate that the graphitic carbon nitride planes are stacking with nanoparticles interlinked by CNTs. The pores are visualized as the repeated tri-s-triazine units of carbon nitride which can be identified as flakes material easily [30,31]. In closer capture, samarium nanoparticles are not observed owing to their small size and well dispersed. Moreover, neodymium nanoparticles, although possesses large sized particles which are incorporated inside the flakes of graphitic carbon nitride and separate particles are not visible in SEM results.

EDX spectra of both Fe_2O_3/g-C_3N_4/CNTs/Nd_2O_3 and Fe_2O_3/g-C_3N_4/CNTs/Sm_2O_3 nanocomposites have been shown in Fig. 5 in which all the nominal components of desired elements are confirmed. 10 μm scales has been used for spotting the EDX sample as evident from Fig. 5.

3.4. Optical studies

The optical studies were completed by using the UV absorbance peaks and tauc plot were plotted as evident in Fig. 6. In this regard, Fe_2O_3/g-C_3N_4/CNTs/Nd_2O_3 and Fe_2O_3/g-C_3N_4/CNTs/Sm_2O_3 NCs were dispersed separately in absolute ethanol with ultra-sonication for 10 min.

The UV absorbance peaks with tauc plot for the calculations of band gap regarding Fe_2O_3/g-C_3N_4/CNTs/Nd_2O_3 and Fe_2O_3/g-C_3N_4/CNTs/Sm_2O_3 NCs can be used for the charge transfer mechanism fruitful for the explanation of photocatalytic efficiency.

The band gap energy values have been calculated using Tauc equation as [32]:

$$\alpha h\nu = A\left(h\nu - E_{obg}\right)^{n} \quad (1)$$

The band gap calculated for neodymium incorporated nanocomposite was 3.5 and 4.0 eV for samarium based nanocomposite respectively.

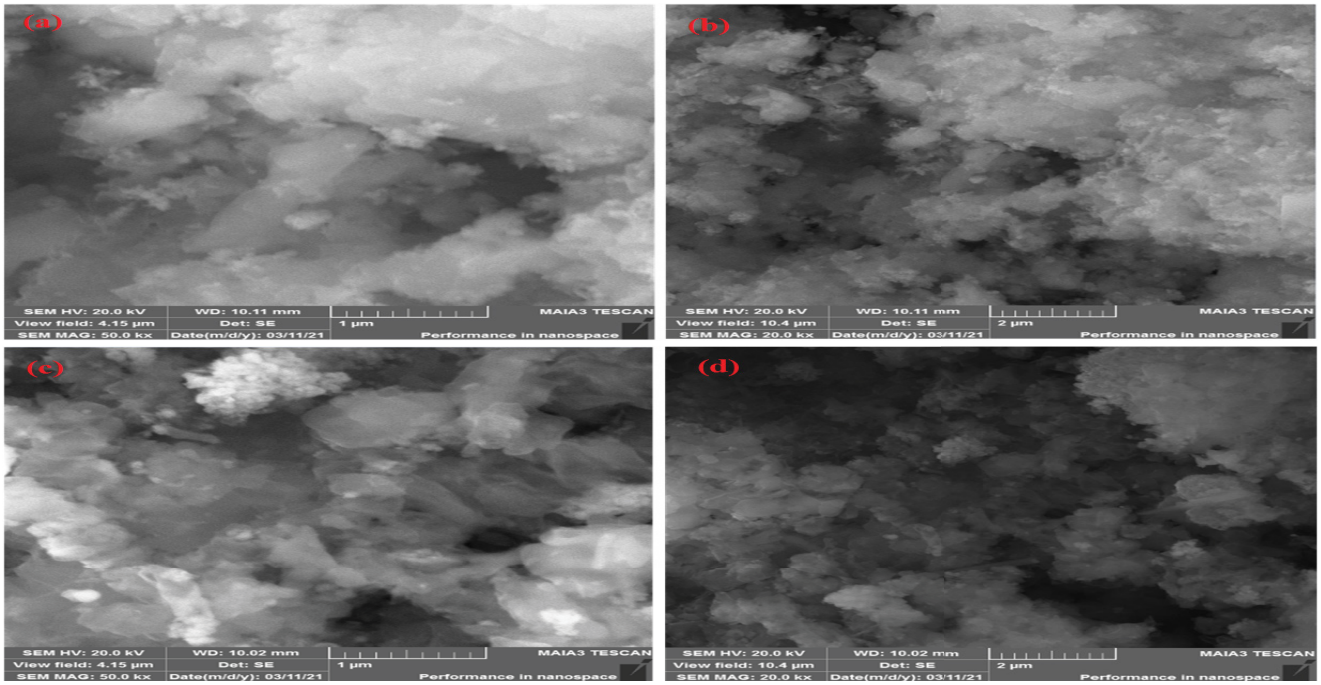

Fig. 4. SEM images of (a, b) Fe_2O_3/g-C_3N_4/CNTs/Nd_2O_3 and (c, d) Fe_2O_3/g-C_3N_4/CNTs/Sm_2O_3 NCs.

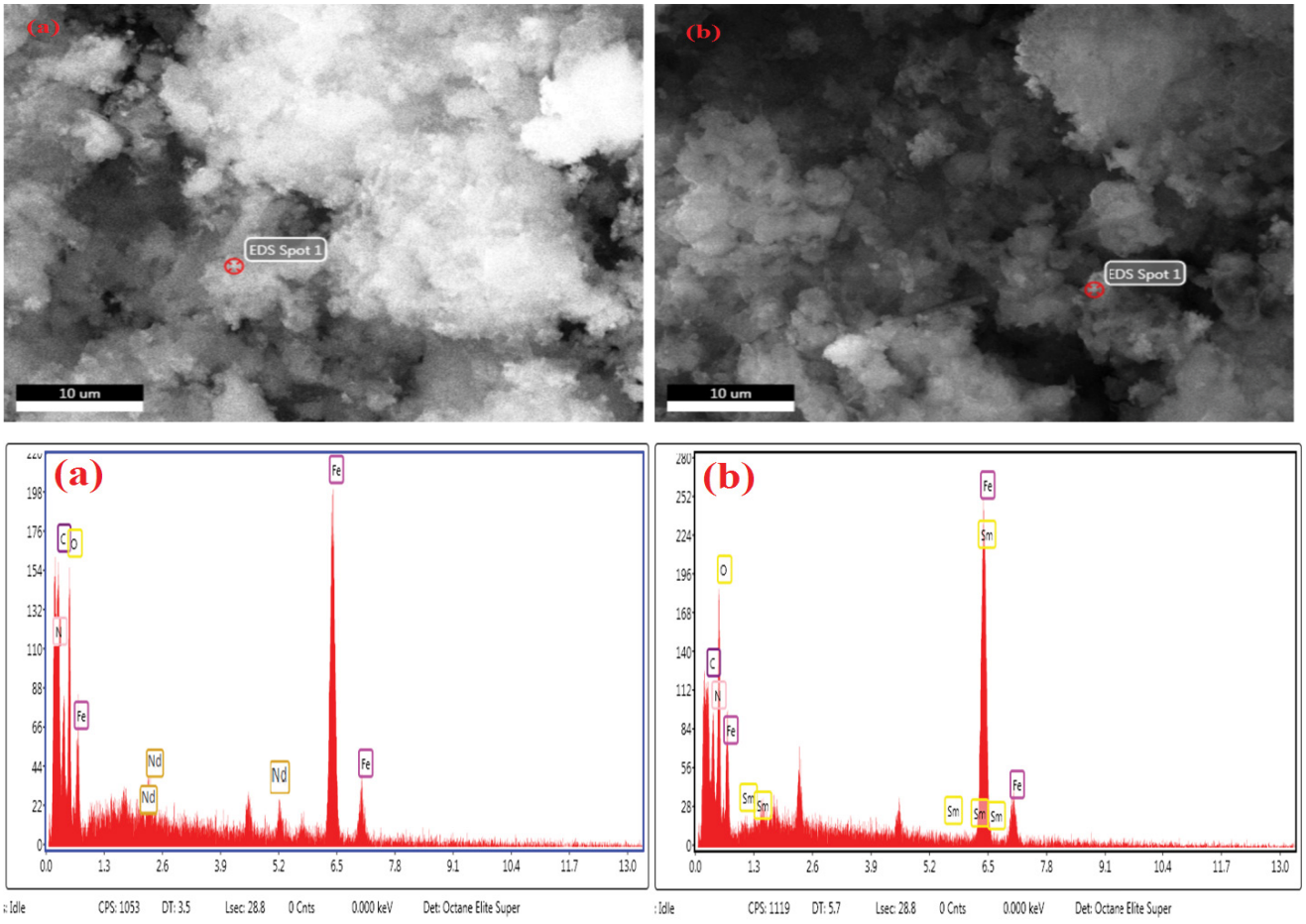

Fig. 5. EDX of (a) Fe_2O_3/g-C_3N_4/CNTs/Nd_2O_3 and (b) Fe_2O_3/g-C_3N_4/CNTs/Sm_2O_3 NCs.

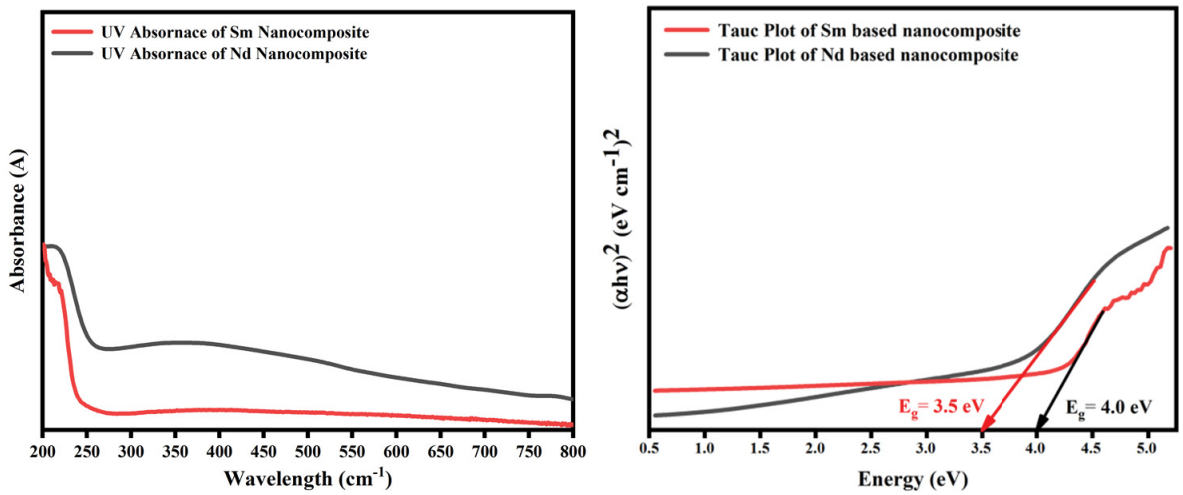

Fig. 6. (a) UV peaks of Fe_2O_3/g-C_3N_4/CNTs/Nd_2O_3 and Fe_2O_3/g-C_3N_4/CNTs/Sm_2O_3 NCs. (b) Tauc plots of Fe_2O_3/g-C_3N_4/CNTs/Nd_2O_3 and Fe_2O_3/g-C_3N_4/CNTs/Sm_2O_3 NCs.

3.5. Photocatalytic degradation of organic dyes

In industry, organic dyes are being used for staining purposes. These days can cause serious environmental problems due to their harmful and cancer causing nature. In this study, two different dyes, Rhodamine B (RhB) which is the member of cationic dye family, 25 ppm of 100 mL was taken, while Congo red (CR) which is the member of anionic dye family, 100 mL of 25 ppm have been utilized as pollutants [33,34]. The photocatalytic degradation of both dyes was observed by using samarium and neodymium based nanocomposites. Results explained in Figs. 7 and 8, show that Fe_2O_3/g-C_3N_4/CNTs/Sm_2O_3 NCs in comparison to Fe_2O_3/g-C_3N_4/CNTs/Nd_2O_3 NCs shows higher photocatalytic activity. Due to electron-hole recombination, least degradation activity is observed in neodymium based composite. Whereas the photocatalytic activity exhibited by Fe_2O_3/g-C_3N_4/CNTs/Sm_2O_3 nanocomposite was high due to the availability of unoccupied 4f energy levels being used by photo electrons thus reduced the recombination pattern of electrons and holes [35,36].

For the deterioration of RhB dye (Fig. 7), the de-ethylation process or cleavage of combined structures results in degradation of dye. The peak position after absorption depicts that the dye remains constant throughout whereas, the absorption intensity decreases with time. Two peaks are shown by the absorption spectrum of Congo red (Fig. 8). One of the bands is at 265 nm that is conjugated with the p-p* transition of aromatic ring structure, while the second band at 432 nm correlates with the n-p transition by lone pair electron which is presented in the nitrogen atom of chromophoric structure present [37,38]. During the reaction, peaks intensities are decreased which indicate that the benzene ring structures were decomposed in Congo red.

The equation used for calculating the percentage degradation of dyes used is [39]. Attained results for degradation of RhB by using neodymium and samarium based nanocomposites are given in Table 1a and 1b while for CR degradation by using neodymium and samarium based nanocomposites are given in Table 1c and 1d.

$$\% D = \frac{\left(A_t - A_o\right)}{A_o} \times 100 \quad (2)$$

3.6. Ion trapping experiments

Various scavengers have been tested for the confirmation of various radicals involved for the degradation of Rhodamine B and Congo red dyes [40]. In ion trapping experiment, 2-propyl alcohol for hydroxyl ions, silver nitrate ($AgNO_3$) for electron capture, Ascorbic acid (Vit.C) for superoxide radicals and EDTA for holes trapping have been adapted and added in the photocatalytic reaction solution as scavengers [36,41].

From the results evident in Fig. 9, it is cleared that the concentration of dye has been considerably decreased from 86.1% to 11.8% in the presence of ascorbic acid, involved in trapping superoxide ions, confirming the main agent for degradation of dye used.

3.7. Control test for photolysis

Control test was performed to check the effect of photolysis using different pHs [42]. The findings of this test were, neural and acidic pHs show minimum/no effect of photolysis due to unavailability of hydroxyl ions within the medium, whereas, when the pH shifted towards basic medium, photolysis shows its dominant effect on dye In current work, the pH for attachment of precursors was set to 3 and the dye solution was of neutral. Therefore, the evidence of photolysis interference during the process of catalytic removal of dyes has been shown in Fig. 10.

3.8. Band structure and proposed mechanism for photocatalytic degradation of dyes

Photocatalysts dye mixtures were irradiated by using visible light emitted from electric bulb placed in closed cabin for dark reaction of 30 min in order to ensure adsorption desorption equilibrium. Fig. 11 shows pictorial illustration of mechanism used for photocatalytic degradation of dyes. Electrons are allowed to excite from

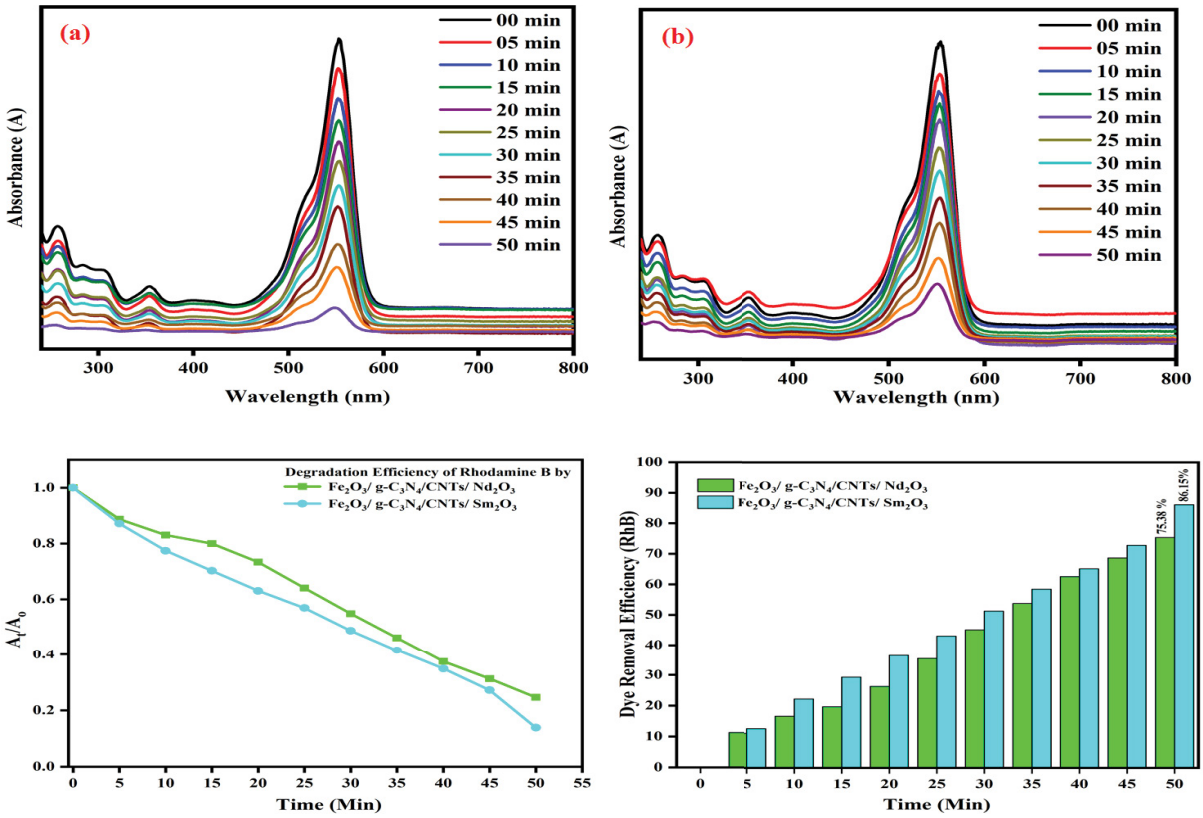

Fig. 7. Photocatalytic degradation of Rhodamine B using (a) Fe_2O_3/g-C_3N_4/CNTs/Nd_2O_3 NCs and (b) Fe_2O_3/g-C_3N_4/CNTs/Sm_2O_3 NCs.

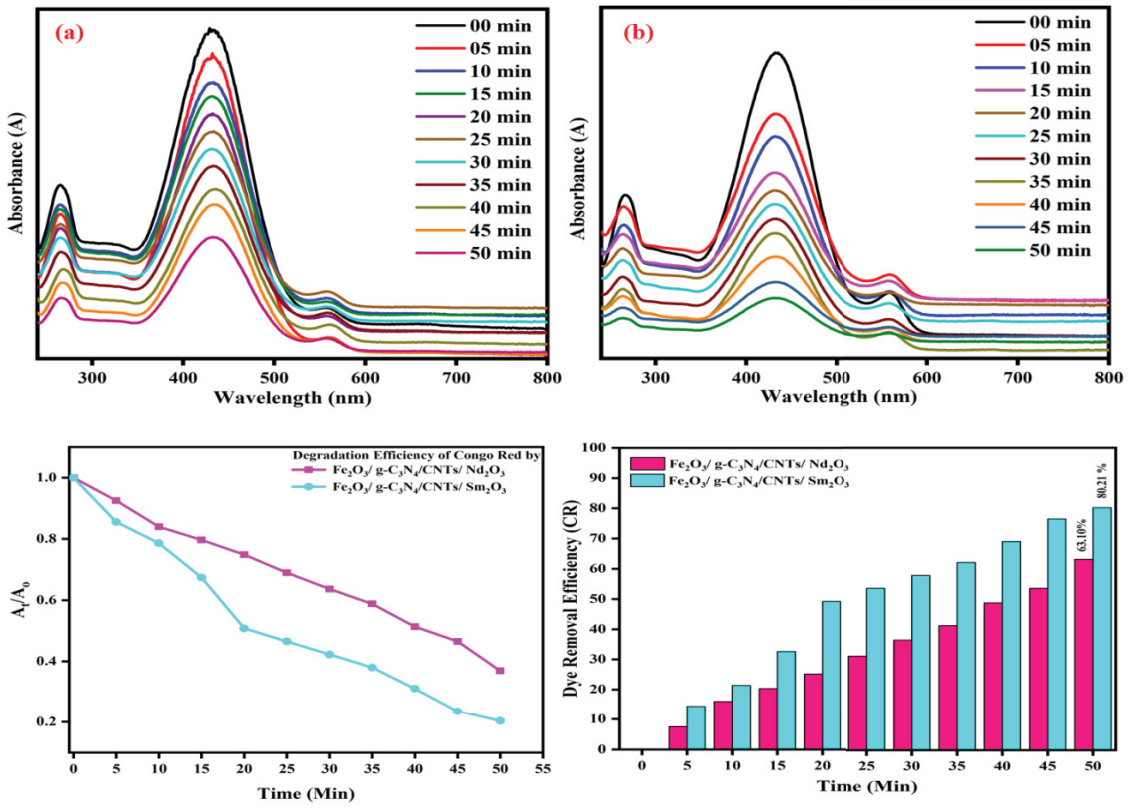

Fig. 8. Photocatalytic degradation of Congo red dyes using (a) Fe_2O_3/g-C_3N_4/CNTs/Nd_2O_3 NCs and (b) Fe_2O_3/g-C_3N_4/CNTs/Sm_2O_3 NCs.

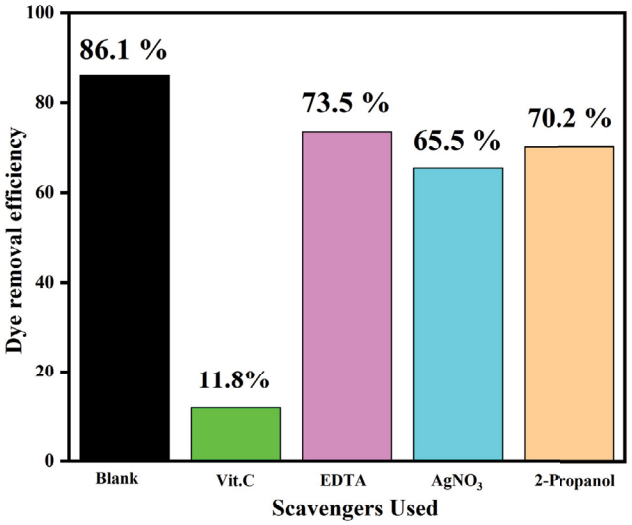

Fig. 9. Removal of RhB dye in the presence of various scavengers.

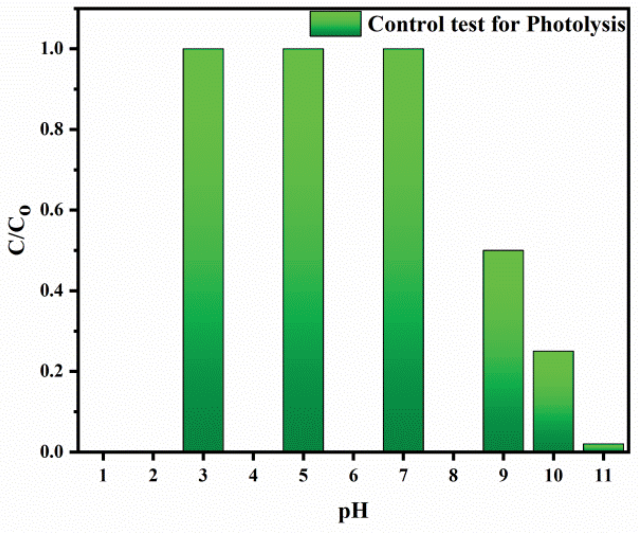

Fig. 10. Control test for photolysis using different pHs.

valance band (VB) to conduction band (CB) when sample is irradiated by light source, as a result; generated electrons and holes cause the degradation of dyes used [39]. It is observed that quantum efficiency is increased due to slow recombination rate of electrons and holes. Reduction of metals is due to the availability of electrons. When oxygen concentration is low within the medium, there is a possibility to store and release oxygen within system. The oxidation state of metals is converted from +2 to +3 states by using oxygen contents, radicals like super oxides also form. Hydroxyl radicals are produced when hydroxyl ions react with photogenerated holes. They can also be formed by the reaction of photogenerated electrons with protons and dissolved oxygen contents [43].

The mechanism involved for degradation of dye using light is shown in equations as:

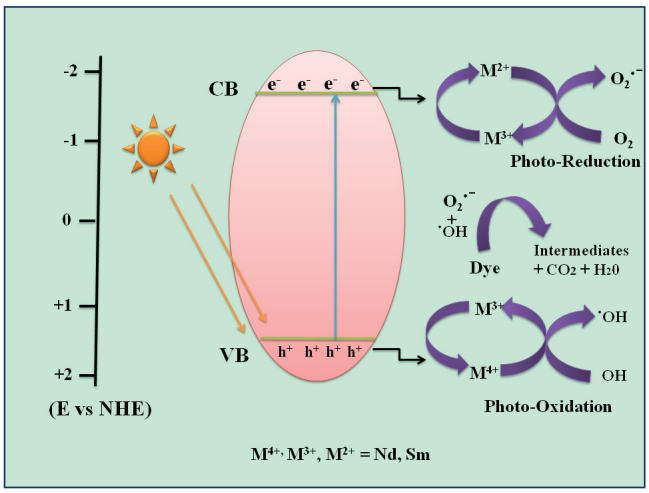

Fig. 11. Pictorial illustration of mechanism used for photocatalytic degradation of dyes.

$$\text{Photocatalyst} + h\nu \rightarrow e^- + h^+ \quad (3)$$

$$M^{3+} + e^- \rightarrow M^{2+} \quad (4)$$

$$M^{3+} + O_2 \rightarrow O_2^- + M^{3+} \quad (5)$$

$$OH^- + h^+ \rightarrow OH^\bullet \quad (6)$$

$$O_2 + e^- \rightarrow O_2^- \quad (7)$$

$$O_2^- + H^+ \rightarrow HO_2^\bullet \quad (8)$$

$$2HO_2 \rightarrow H_2O_2 + O_2 \quad (9)$$

Table 2 depicts the comparison of degradation performance of different photocatalysts using different dyes, time consumed and % removal of dyes as efficiency along with references.

4. Conclusions

The graphitic carbon nitride based neodymium and samarium nanocomposites incorporated with CNTs were prepared using thermal exfoliation, co-precipitation and ultra-sonication methods respectively. SEM and EDX results confirmed the flaked morphological of as-synthesized nanocomposites of Fe_2O_3/g-C_3N_4/CNTs/Nd_2O_3 and Fe_2O_3/g-C_3N_4/CNTs/Sm_2O_3 respectively. The UV-Visible studies confirmed the shift of absorption band towards longer wavelength thus confirming the shortened band gap of g-C_3N_4 as main precursor for photocatalytic applications. The results with degradation efficiency of 75.3% using RhB and 63.1% using Congo red has been calculated for Fe_2O_3/g-C_3N_4/CNTs/Nd_2O_3 nanocomposite while 86.15% for RhB and 80.2% for Congo red dye has been recorded using Fe_2O_3/g-C_3N_4/CNTs/Sm_2O_3 respectively. The scavenger's test confirmed that superoxide as main agent for degrading the dyes. The

Table 2
Comparison of degradation efficiency of different catalysts using Congo red and Rhodamine B dyes

Photocatalyst used	Quantity (mg)	Dyes used	Removal (%)	Time used (min)	References
Fe_2O_3/g-C_3N_4	01	RhB (Rhodamine B)	90	120	[44]
TiO_2/g-C_3N_4	10	RhB (Rhodamine B)	80	300	[45]
ZnO/MWCNTs	20	MO (Methyl orange)	80.2	60	[46]
Nd-TiO_2-GO	20	IC (Indigo carmine)	92	180	[47]
Fe_2O_3/C_3N_4/CNTs/Sm_2O_3	05	RhB (Rhodamine B)	86.1	50	Present Work
		CR (Congo red)	80.2	50	

efficient removal of RhB and CR dyes using samarium based nanocomposite is higher as compared to that of neodymium based nanocomposite, thus confirming the better choice of photocatalysts as comparitive study between neodymium based and samarium based nanocomposites.

Acknowledgements

The authors are highly thankful to Islamia University of Bahawalpur (IUB) and Higher Education commission (HEC) of Pakistan for financial support.

References

[1] X. Huang, F. Guo, M. Li, H. Ren, Y. Shi, L. Chen, Hydrothermal synthesis of $ZnSnO_3$ nanoparticles decorated on g-C_3N_4 nanosheets for accelerated photocatalytic degradation of tetracycline under the visible-light irradiation, Sep. Purif. Technol., 230 (2020) 115854, doi: 10.1016/j.seppur.2019.115854.
[2] H. Wang, Z. Jin, R. Gan, S. Min, J. Xu, Novel strategy of defect-induced graphite nitride carbon preparation and photocatalytic performance, Catal. Lett., 148 (2018) 1296–1308.
[3] G. Liao, Y. Gong, L. Zhang, H. Gao, G.-J. Yang, B. Fang, Semiconductor polymeric graphitic carbon nitride photocatalysts: the "holy grail" for the photocatalytic hydrogen evolution reaction under visible light, Energy Environ. Sci., 12 (2019) 2080–2147.
[4] N.T.T. Truc, T.-D. Pham, M.V. Nguyen, D. Van Thuan, P. Thao, H.T. Trang, D.T. Tran, D.N. Minh, N.T. Hanh, H.M. Ngoc, Advanced $NiMoO_4$/g-C3N_4 Z-scheme heterojunction photocatalyst for efficient conversion of CO_2 to valuable products, J. Alloys Compd., 842 (2020) 155860, doi: 10.1016/j.jallcom.2020.155860.
[5] S. Kumar, A. Baruah, S. Tonda, B. Kumar, V. Shanker, B. Sreedhar, Cost-effective and eco-friendly synthesis of novel and stable N-doped ZnO/gC_3N_4 core–shell nanoplates with excellent visible-light responsive photocatalysis, Nanoscale, 6 (2014) 4830–4842.
[6] M. Rakibuddin, H. Kim, Samarium(III)-doped ZnO/graphitic–C_3N_4 composites for enhanced hydrogen generation from water under visible light photocatalysis, J. Alloys Compd., 832 (2020) 154887, doi: 10.1016/j.jallcom.2020.154887.
[7] R. Ahmad, N. Tripathy, A. Khosla, M. Khan, P. Mishra, W.A. Ansari, M.A. Syed, Y.-B. Hahn, Recent advances in nanostructured graphitic carbon nitride as a sensing material for heavy metal ions, J. Electrochem. Soc., 167 (2019) 037519.
[8] D. Monga, D. Ilager, N.P. Shetti, S. Basu, T.M. Aminabhavi, 2D/2d heterojunction of MoS_2/g-C_3N_4 nanoflowers for enhanced visible-light-driven photocatalytic and electrochemical degradation of organic pollutants, J. Environ. Manage., 274 (2020) 111208, doi: 10.1016/j.jenvman.2020.111208.
[9] B. Klahr, S. Gimenez, F. Fabregat-Santiago, T. Hamann, J. Bisquert, Water oxidation at hematite photoelectrodes: the role of surface states, J. Am. Chem. Soc., 134 (2012) 4294–4302.
[10] Y. Geng, D. Chen, N. Li, Q. Xu, H. Li, J. He, J. Lu, Z-Scheme 2D/2D α-Fe_2O_3/g-C_3N_4 heterojunction for photocatalytic oxidation of nitric oxide, Appl. Catal., B, 280 (2021) 119409, doi: 10.1016/j.apcatb.2020.119409.
[11] K.T. Kubra, R. Sharif, B. Patil, A. Javaid, S. Shahzadi, A. Salman, S. Siddique, G. Ali, Hydrothermal synthesis of neodymium oxide nanoparticles and its nanocomposites with manganese oxide as electrode materials for supercapacitor application, J. Alloys. Compd., 815 (2020) 152104, doi: 10.1016/j.jallcom.2019.152104.
[12] S. Ahmadi, L. Mohammadi, A. Rahdar, S. Rahdar, R. Dehghani, C. Adaobi Igwegbe, G.Z. Kyzas, Acid dye removal from aqueous solution by using neodymium(III) oxide nanoadsorbents, Nanomaterials, 10 (2020) 556, doi: 10.3390/nano10030556.
[13] R. James, Electrical Properties of La_2CuO_4 and Nd_2CuO_4 and Their Coexistent p-n Heterojunction, University of Oslo, 2020.
[14] K. Narasimharao, T.T. Ali, Influence of synthesis conditions on physico-chemical and photocatalytic properties of rare earth (Ho, Nd and Sm) oxides, J. Mater. Res. Technol., 9 (2020) 1819–1830.
[15] S. Mallakpour, E. Khadem, Carbon nanotube–metal oxide nanocomposites: fabrication, properties and applications, Chem. Eng. J., 302 (2016) 344–367.
[16] M. Farahmandjou, F. Soflaee, Synthesis and characterization of α-Fe_2O_3 nanoparticles by simple co-precipitation method, Phys. Chem. Res., 3 (2015) 191–196.
[17] Z. Wang, Y. Huo, Y. Fan, R. Wu, H. Wu, F. Wang, X. Xu, Facile synthesis of carbon-rich g-C_3N_4 by copolymerization of urea and tetracyanoethylene for photocatalytic degradation of Orange II, J. Photochem. Photobiol., A, 358 (2018) 61–69.
[18] S. Zinatloo-Ajabshir, S. Mortazavi-Derazkola, M. Salavati-Niasari, Sonochemical synthesis, characterization and photodegradation of organic pollutant over Nd_2O_3 nanostructures prepared via a new simple route, Sep. Purif. Technol., 178 (2017) 138–146.
[19] T.A. Nguyen, V. Pham, T.L. Pham, L.T.T. Nguyen, I.Y. Mittova, V. Mittova, L.N. Vo, B.T.T. Nguyen, V.X. Bui, E. Viryutina, Simple synthesis of $NdFeO_3$ nanoparticles by the co-precipitation method based on a study of thermal behaviors of Fe(III) and Nd(III) hydroxides, Crystals, 10 (2020) 219, doi: 10.3390/cryst10030219.
[20] L. Zhou, L. Wang, J. Zhang, J. Lei, Y. Liu, Well-dispersed Fe_2O_3 nanoparticles on g-C_3N_4 for efficient and stable photo-fenton photocatalysis under visible-light irradiation, Eur. J. Inorg. Chem., 2016 (2016) 5387–5392.
[21] X. Zhang, L. Hao, Preparation and catalytic activity of M_2O_3/CNTs (M = Y, Nd, Sm) nanocomposites by solvothermal process, J. Nanomater., 2018 (2018) 3635164, doi: 10.1155/2018/3635164.
[22] B. Zhaorigetu, G. Ridi, L. Min, Preparation of Nd_2O_3 nanoparticles by tartrate route, J. Alloys Compd., 427 (2007) 235–237.
[23] S. Sobhanardakani, A. Jafari, R. Zandipak, A. Meidanchi, Removal of heavy metal (Hg(II) and Cr(VI)) ions from aqueous solutions using Fe_2O_3@SiO_2 thin films as a novel adsorbent, Process Saf. Environ. Prot., 120 (2018) 348–357.
[24] Y. Yang, L. Geng, Y. Guo, J. Meng, Y. Guo, Easy dispersion and excellent visible-light photocatalytic activity of the ultrathin

urea-derived g-C_3N_4 nanosheets, Appl. Surf. Sci., 425 (2017) 535–546.
[25] X. Zheng, Y. Hu, Z. Li, Y. Dong, J. Zhang, J. Wen, H. Peng, Sm_2O_3 nanoparticles coated with N-doped carbon for enhanced visible-light photocatalysis, J. Phys. Chem. Solids, 130 (2019) 180–188.
[26] T. Belin, F. Epron, Characterization methods of carbon nanotubes: a review, Mater. Sci. Eng., B, 119 (2005) 105–118.
[27] J. Liu, T. Zhang, Z. Wang, G. Dawson, W. Chen, Simple pyrolysis of urea into graphitic carbon nitride with recyclable adsorption and photocatalytic activity, J. Mater. Chem., 21 (2011) 14398–14401.
[28] T. Liu, Y. Zhang, H. Shao, X. Li, Synthesis and characteristics of Sm_2O_3 and Nd_2O_3 nanoparticles, Langmuir, 19 (2003) 7569–7572.
[29] P. Ghosh, S. Kundu, A. Kar, K. Ramanujachary, S. Lofland, A. Patra, Synthesis and characterization of different shaped Sm_2O_3 nanocrystals, J. Phys. D: Appl. Phys., 43 (2010) 405401.
[30] L. Li, H. Yu, J. Xu, S. Zhao, Z. Liu, Y. Li, Rare earth element, Sm, modified graphite phase carbon nitride heterostructure for photocatalytic hydrogen production, New J. Chem., 43 (2019) 1716–1724.
[31] J. He, F. Qiu, Q. Xu, J. An, R. Qiu, A carbon nanofibers–Sm_2O_3 nanocomposite: a novel electrochemical platform for simultaneously detecting two isomers of dihydroxybenzene, Anal. Methods, 10 (2018) 1852–1862.
[32] N. Masunga, B.B. Mamba, K.K. Kefeni, Trace samarium doped graphitic carbon nitride photocatalytic activity toward metanil yellow dye degradation under visible light irradiation, Colloids Surf., A, 602 (2020) 125107, doi: 10.1016/j.colsurfa.2020.125107.
[33] M. Alaei, A.R. Mahjoub, A. Rashidi, Effect of WO_3 nanoparticles on Congo red and Rhodamine B photo degradation, Iran. J. Chem. CHem. Eng., 31 (2012) 23–29.
[34] N. Farooq, R. Luque, M.M. Hessien, A.M. Qureshi, F. Sahiba, M.A. Nazir, A comparative study of cerium-and ytterbium-based GO/g-C_3N_4/Fe_2O_3 composites for electrochemical and photocatalytic applications, Appl. Sci., 11 (2021) 9000, doi: 10.3390/app11199000.
[35] P. Pascariu, C. Cojocaru, N. Olaru, P. Samoila, A. Airinei, M. Ignat, L. Sacarescu, D. Timpu, Novel rare earth (RE-La, Er, Sm) metal doped ZnO photocatalysts for degradation of Congo red dye: synthesis, characterization and kinetic studies, J. Environ. Manage., 239 (2019) 225–234.
[36] J. Thomas, K. Ambili, S. Radhika, Synthesis of Sm^{3+}-doped graphitic carbon nitride nanosheets for the photocatalytic degradation of organic pollutants under sunlight, Catal. Today, 310 (2018) 11–18.
[37] A.A. Wani, A.M. Khan, Y.K. Manea, M.A. Salem, Enhanced photocatalytic degradation of organic dyes from aqueous environment using neodymium-doped mesoporous layered double hydroxide, J. Rare Earths, (2021), doi: 10.1016/j.jre.2021.09.007 (in Press).
[38] Z.H. Mahmoud, R. Adham AL-Bayati, A.A. Khadom, Visible-Light Degradation of Rhodamine B Dye by Samarium Modified Anatase Titanium Dioxide (Sm-TiO_2): Structural, Characterization, Optical and Electrochemical Studies, SSRN, 2021.
[39] N. Farooq, A. ur Rehman, A.M. Qureshi, Z. ur Rehman, A. Ahmad, M.K. Aslam, H.M.A. Javed, S. Hussain, M.A. Habila, N. AlMasoud, Au@GO@g-C_3N_4 and Fe_2O_3 nanocomposite for efficient photocatalytic and electrochemical applications, Surf. Interfaces, 26 (2021) 101399, doi: 10.1016/j.surfin.2021.101399.
[40] O.P. Kumar, M.N. Ashiq, S.S.A. Shah, S. Akhtar, M.A. Al Obaidi, I.M. Mujtaba, A. ur Rehman, Nanoscale ZrRGOCuFe layered double hydroxide composites for enhanced photocatalytic degradation of dye contaminant, Mater. Sci. Semicond. Process., 128 (2021) 105748, doi: 10.1016/j.mssp.2021.105748.
[41] M. Jourshabani, Z. Shariatinia, A. Badiei, Synthesis and characterization of novel Sm_2O_3/S-doped g-C_3N_4 nanocomposites with enhanced photocatalytic activities under visible light irradiation, Appl. Surf. Sci., 427 (2018) 375–387.
[42] A.H. Jawad, N.S.A. Mubarak, M.A.M. Ishak, K. Ismail, W.I. Nawawi, Kinetics of photocatalytic decolourization of cationic dye using porous TiO_2 film, J. Taibah Univ. Sci., 10 (2016) 352–362.
[43] I. Paramasivam, H. Jha, N. Liu, P. Schmuki, A review of photocatalysis using self-organized TiO_2 nanotubes and other ordered oxide nanostructures, Small, 8 (2012) 3073–3103.
[44] H. Zhang, C. Zhu, J. Cao, Q. Tang, M. Li, P. Kang, C. Shi, M. Ma, Ultrasonic-assisted synthesis of 2D α-Fe_2O_3@g-C_3N_4 composite with excellent visible light photocatalytic activity, Catalysts, 8 (2018) 457, doi: 10.3390/catal8100457.
[45] X. Lu, Q. Wang, D. Cui, Preparation and photocatalytic properties of g-C_3N_4/TiO_2 hybrid composite, J. Mater. Sci. Technol., 26 (2010) 925–930.
[46] C. Chen, T. Liu, L. Lin, X. Xie, X. Chen, Q. Liu, B. Liang, W. Yu, C. Qiu, Multi-walled carbon nanotube-supported metal-doped ZnO nanoparticles and their photocatalytic property, J. Nanopart. Res., 15 (2013) 1–9.
[47] S.O.-B. Oppong, W.W. Anku, S.K. Shukla, E.S. Agorku, P.P. Govender, Photocatalytic degradation of indigo carmine using Nd-doped TiO_2-decorated graphene oxide nanocomposites, J. Sol-Gel Sci. Technol., 80 (2016) 38–49.